

Whisker-Inspired Tactile Sensing for Bumper Drone

By

Supa, Pongporn

MSc Robotics Dissertation



School of Engineering Mathematics and Technology
UNIVERSITY OF BRISTOL
&
Department of Engineering Design and Mathematics
UNIVERSITY OF THE WEST OF ENGLAND

A MSc dissertation submitted to the University of Bristol and the
University of the West of England in accordance with the
requirements of the degree of MASTER OF SCIENCE IN ROBOTICS
in the Faculty of Engineering.

September 4, 2025

Declaration of own work

I declare that the work in this MSc dissertation was carried out in accordance with the requirements of the University's Regulations and Code of Practice for Research Degree Programmes and that it has not been submitted for any other academic award. Except where indicated by specific reference in the text, the work is the candidate's own work. Work done in collaboration with, or with the assistance of, others, is indicated as such. Any views expressed in the dissertation are those of the author.

Pongporn Supa, 29 Aug 2025

Ethics statement

To fill in according to the Dissertation Handbook Section 3.2.

Pongporn Supa, 29 Aug 2025

Whisker-Inspired Tactile Sensing for Bumper Drone

Pongporn Supa

Abstract—Aerial robots have shifted their applications from passive observation to active physical interaction with the environment in risk-prone tasks for human workers. Previous research has successfully demonstrated their capabilities in manipulation tasks with minimal attention to tactile navigation. This task typically involves push-and-slide operations affected by friction forces upon contact with unknown surfaces. While many studies focus on handling friction forces, this work takes a different approach by performing repeated, brief contacts called touch-and-go manoeuvres, enabling aerial robots to use tactile feedback for navigation. The challenge in this behaviour lies in the ability to recover from collisions. Inspired by nature, we designed a whisker-inspired drone bumper that passively recovers from collisions and performs such flying behaviour with minimal control. We propose a real-time preprocessing method to mitigate the inherent nonlinearity, hysteresis, and creep effects of our soft whisker sensor design. By combining biomimetic whisker morphology with flying insect reflex-landing behaviour, we demonstrate self-recovery mechanisms where our whisker design acts as an embodied mass-spring-damper system. Experiments show that our bumper drone can absorb impact energy from collisions while maintaining vehicle stability, achieving minimal attitude disturbances with pitch oscillations of only 4° and roll oscillations of just 0.74° . Additionally, the bumper drone can maintain its stability while applying sustained normal contact force with the vertical wall.

I. INTRODUCTION

Unmanned Aerial Vehicles (UAVs) are undergoing a paradigm shift from passive observation to active physical interaction with the external environment. This transformation has unlocked new possibilities for Aerial Physical Interaction (APhI), particularly in high-risk operations such as inspection and maintenance of wind turbines, bridges, and high-voltage power lines where human operations are dangerous and time-consuming [1]. By attaching rigid or articulated end-effectors to aerial platforms, researchers have developed aerial manipulators capable of intentionally interacting with the environment to perform diverse manipulation tasks. Recent APhI research has demonstrated successful aerial manipulation across various scenarios, including object pushing [2], emergency switch activation [3], grasping [4], [5], contact-based inspection [6], [7], [8], and aerial calligraphy [9].

However, few studies have explored leveraging these physical interaction capabilities for navigation purposes [10], [11]. In challenging environments where traditional sensors such as LiDAR or cameras perform poorly due to limited visibility (smoke, fog, dust, or complete darkness), direct environmental contact offers an alternative sensing modality. This approach, known as Tactile Navigation (TN) [11], enables aerial manipulators to estimate their location and orientation relative to contacted surfaces, similar to how

nocturnal or vision-impaired animals navigate through touch.

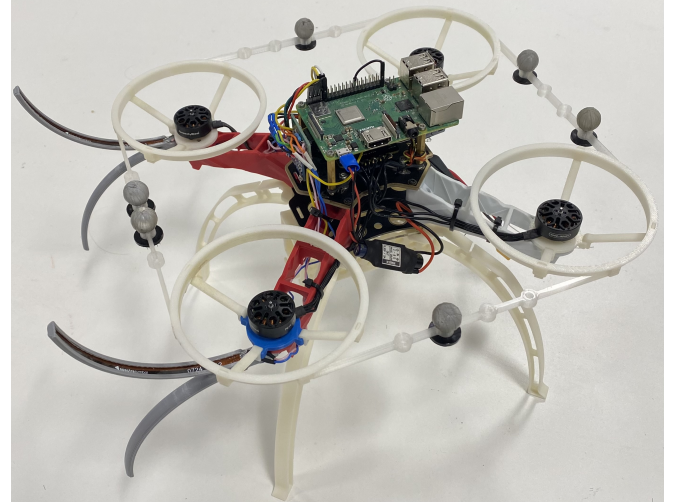


Fig. 1. Whisker-inspired bumper drone: a 700g flying robot that can exert force on objects and have self-recovery mechanism after collisions.

Achieving effective TN requires aerial manipulators to maintain vehicle stability during continuous contact while managing varying friction forces from different surface textures. Current approaches address these challenges through various strategies. In [8], an axis-selective impedance control is proposed to compensate for directional disturbances, including friction forces, by adjusting impedance parameters. A hybrid motion-force controller that incorporates both normal and friction forces into contact wrench models has been studied for time-varying contact force [9]. While effective, these approaches require omnidirectional platforms and expensive Force-Torque (F/T) sensors, significantly increasing system weight and control complexity. Alternatively, several studies propose compliant end-effector designs that can assume single-point contact and minimise friction through careful material selection and morphology, such as PLA spherical fingertips [11] and metal ball casters [10]. However, these approaches remain sensitive to small contact force variations that compromise surface orientation estimation accuracy.

Inspired by nature, we propose a novel solution that overcomes friction forces during navigation through touch-and-go manoeuvre. By controlling under-actuated aerial manipulators to perform brief, repeated contacts with surfaces like flying insects, we eliminate the need for continuous sliding and friction force compensation while enabling exploration of unknown environments. To achieve such flying behaviour, we design a novel whisker-inspired bumper drone

(Figure 1) that provides self-recovery mechanisms from collision passively. Our design can function as a mass-spring-damper system to protect the aerial robot's structure. While many studies have proposed collision-resilient aerial platforms using carbon fibres cage [12] or shock absorber [13] to absorb collision energy, these approaches typically lack manipulation capabilities and fail to detect collisions when colliding at low speed or on soft obstacles.

By mounting flex sensors on our whisker sensors, we can estimate normal contact force and displacement through deformation. By controlling pitch motion of UAVs, we demonstrate that our platform can apply substantial normal contact force to environment and remain stable after physical interaction without any control strategy. To the best of our knowledge, this work represents the first integration of force-sensing elements and control algorithms into a unified morphological design for aerial robots, advancing toward Embodied Aerial Physical Interaction (E-APhI) [14]. We demonstrate that morphological intelligence can simplify control complexity, transforming traditional impedance control problems or LQR-based approaches into orientation tracking tasks. Furthermore, we validate that standard low-level controllers can maintain stability during physical contact operations, enabling both tactile navigation and static manipulation tasks.

The contributions of this study are listed below:

- We design and build a whisker-inspired bumper drone capable of both static object pushing tasks and tactile navigation operations.
- We perform morphological analysis of our whisker design and propose a real-time signal processing approach that mitigates vibration, hysteresis, and creep effects inherent in soft material deformation under mechanical stress.
- We validate a touch-and-go maneuver inspired by flying insects that repeatedly contact obstacles until finding escape routes for tactile navigation. This approach eliminates the need for friction force compensation from our system and demonstrates that our design, using only standard low-level controllers of aerial vehicles, can maintain vehicle stability during sustained contact with a vertical wall.

II. WHISKER DESIGN AND FABRICATION

A. Conceptual Design

In biological systems, whiskers enable safe physical interaction with the environment through mechanoreception at their follicle base. Upon contact, forces and moments transmitted through the whisker shaft cause follicle deformation that mechanoreceptors convert into neural signals for processing and behavioural response. This bio-inspired tactile sensing provides an alternative approach to force measurement during physical interaction that is lightweight, highly sensitive, and eliminates reliance on expensive force-torque sensors whose structural housing requirements significantly increase system weight.

Many researchers have implemented whisker-based sensing using MEMS barometers [15], fibre Bragg grating (FBG) sensors [16], Hall effect sensors [17], etc., for contact detection. However, these approaches involve delicate manufacturing processes and are primarily designed for contact point localisation where contact forces are insufficient for manipulation tasks. Our work focuses on contact detection and force measurement at the contact point suitable for aerial physical interaction applications, providing a cost-effective sensing solution that is easy to reproduce.

Our whisker sensor design consists of two main parts: 1) flex sensors directly measuring whisker deformation; 2) whisker housing design serving as a spring-damping system to absorb impact energy. The sensor housing utilises flexible 3D printing with TPU material. Our whisker housing design is fabricated using a Bambu Lab A1 printer with TPU for AMS which has a Shore hardness of 68D, configuring the printing parameters with no infill density using a 0.6 mm nozzle. The flex sensors are placed inside the 3D-printed housing that is curved to ensure consistent bending direction when making contact with surfaces, as shown in Figure 2c. The mass of the whisker is only 7g.

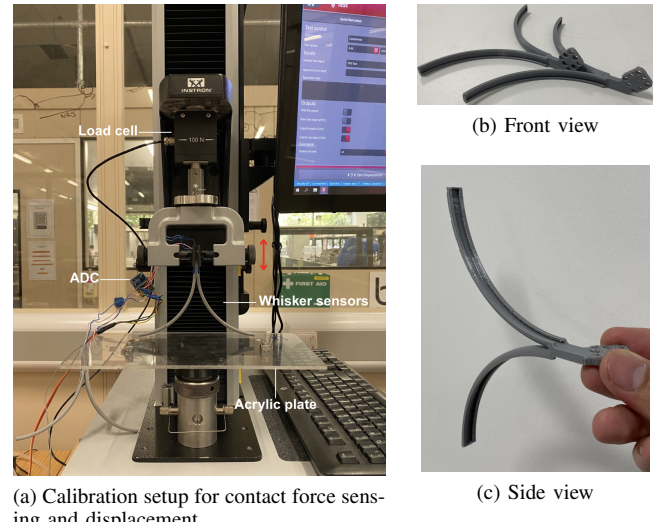


Fig. 2. Experimental setup and whisker design. (a) Instron testing machine setup for calibration with compression direction indicated. (b) Front view and (c) side view of the 3D printed whisker sensors.

In traditional whisker sensing, researchers use Nitinol wires as shafts in their designs to minimise friction forces upon interaction [15], [17], [16]. However, our approach diverges from the conventional sliding-contact approach by implementing a touch-and-go navigation strategy that necessitates robust collision recovery mechanisms inspired by flying insect behaviour.

Flying insects demonstrate remarkable collision resilience through a behavioral repertoire. When they collide with vertical walls using their heads, they extend their legs to decelerate and dampen the impact through a mechanism known as *reflex-landing*, which provides controlled wall rebound and post-collision stability [18]. Drawing from this biological analogy, we arrange four whisker sensors in a

biomimetic arrangement with two upper sensors (analogous to an insect head) and two lower sensors (analogous to insect legs) for damping and stabilisation (Figure 2).

Our collision dynamics hypothesis centres on sequential contact mechanics. Initial surface contact occurs through the upper whisker pair, generating reaction forces that produce positive pitch moments and corresponding positive pitch velocities during wall rebound. Subsequently, the lower whiskers engage the surface, functioning as a damping system that simultaneously dissipates impact energy and generates counteracting negative pitch moments, facilitating passive bounce-off behavior.

This design aligns with principles of insect post-collision flight, where body posture stabilisation takes precedence over trajectory control [18]. Our experimental validation confirms that collision recovery occurs passively through the inherent morphology of the whisker sensor configuration and pitch angle correction, successfully replicating the collision strategies observed in flying insects.

B. Whisker Characteristic

We analysed our whisker sensor morphology to establish the relationship between resistance and contact force/displacement using systematic calibration methods. The experimental setup employed an Instron tensile testing machine in compression mode to simultaneously measure force and displacement while pressing whiskers against an acrylic plate (Figure 2a). Prior testing was performed to find the maximum operational force of 10N for single-sided whisker sensors (comprising 2 flex sensors) before permanent damage or structural failure occurs. Since each flex sensor exhibits different resistance readings in its unbent state (zero deformation), a calibration signal is essential to account for these inherent baseline variations. We collected 1000 resistance samples from each sensor while unbent, calculated their mean values, and subtracted baseline values from all subsequent resistance readings before each trial. This calibrated baseline resistance is denoted as $\Omega_{i,0}$.

Subsequently, we performed whisker levelling by placing thin paper above the acrylic plate and adjusting the height of the whisker sensor placement until the measured force from the load cell exceeded zero. We set this point as our initial reference where both displacement and force were set to zero. One experimental trial consisted of loading and unloading phases: compression from 0 N to 10 N followed by release back to 0mm displacement, both at identical compression rates. We used zero displacement as the stopping criterion for our experimental trials to determine whether our flexible sensors exhibit creep effects. Compression rates of 10mm/min and 100mm/min were used, with five repetition cycles per rate, yielding 10 complete datasets. The calibration assumes symmetric behaviour between upper and lower whiskers, distributing the 10N maximum force equally (5N per whisker pair).

As shown in Figure 3a, the flexible whisker sensors demonstrate non-linear responses and hysteresis at both compression rates in force and displacement measurements.

At the 10mm/min compression rate, resistance initially increases from approximately $63\,000\Omega$ to $63\,900\Omega$ as applied force increases from 0N to 0.9N. However, beyond this point, resistance begins to decrease progressively at (0.9N, 14mm), termed the transition point. Throughout the loading phase, as force continues to increase, resistance gradually decreases to approximately $59\,400\Omega$ at (5N, 40mm). During the unloading phase, as force decreases from 5N, resistance initially increases but exhibits a different trajectory, creating a hysteresis loop. The transition point occurs at lower contact force but higher displacement (0.6N, 22mm). Finally, the resistance reading does not return to the original baseline, ending at approximately $62\,600\Omega$ at a displacement value of 6mm, demonstrating the creep effect of the whisker sensors.

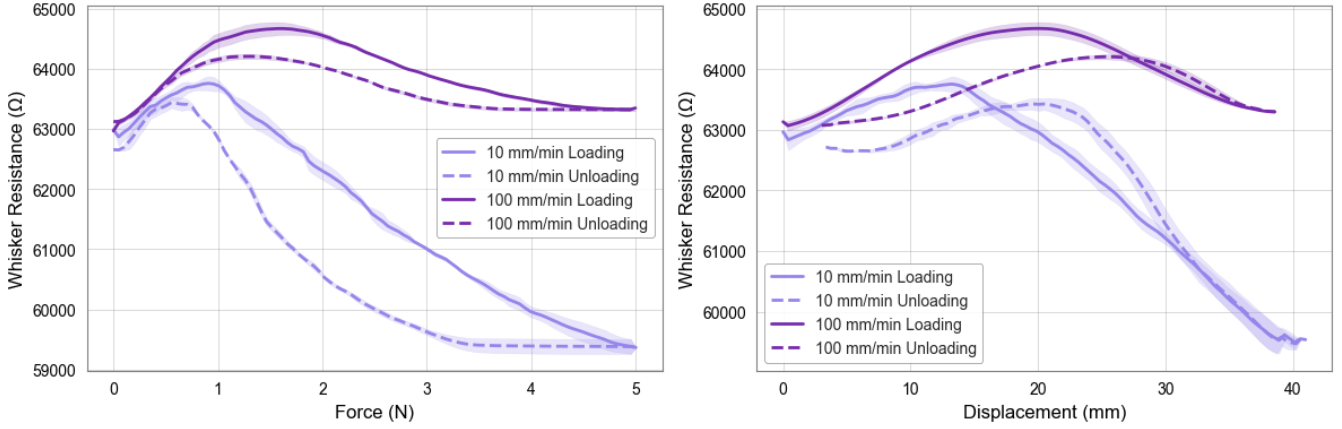
At the faster 100mm/min compression rate, this behaviour is significantly modified. The resistance exhibits a smoother response, increasing from $63\,000\Omega$ to approximately $64\,500\Omega$ as force increases. The transition point occurs at higher contact force and higher displacement around (1.5N, 20mm) compared to the 10mm/min compression rate. Beyond this point, resistance begins to gradually decrease to $63\,500\Omega$ at (5N, 38mm). During the unloading phase, the transition point is closer to that of the loading phase at (1.2N, 27mm), the hysteresis loop is considerably smaller, and the unloading path more closely follows the loading trajectory. However, the final displacement shows the same value as the 10mm/min compression rate at 6mm.

The results reveal significant velocity-dependent behaviour, where increases in approaching velocity cause hysteresis loops to become smaller and shift the transition point towards higher contact forces. At slower compression rates (10mm/min), the whisker sensors exhibit pronounced non-linear responses with large hysteresis loops and early transition points at low forces, making accurate force estimation challenging. Conversely, at faster compression rates (100mm/min), the sensor response becomes more predictable with reduced hysteresis and delayed transition points. In Section III, since our collisions occur rapidly, the resistance increases predictably when contact force increases, similar to the faster compression rate behaviour. However, for applications requiring precise force measurement across varying contact velocities, particularly at lower speeds, the non-linearity and hysteresis effects observed at slow compression rates must be addressed through appropriate signal processing techniques to ensure reliable sensor performance.

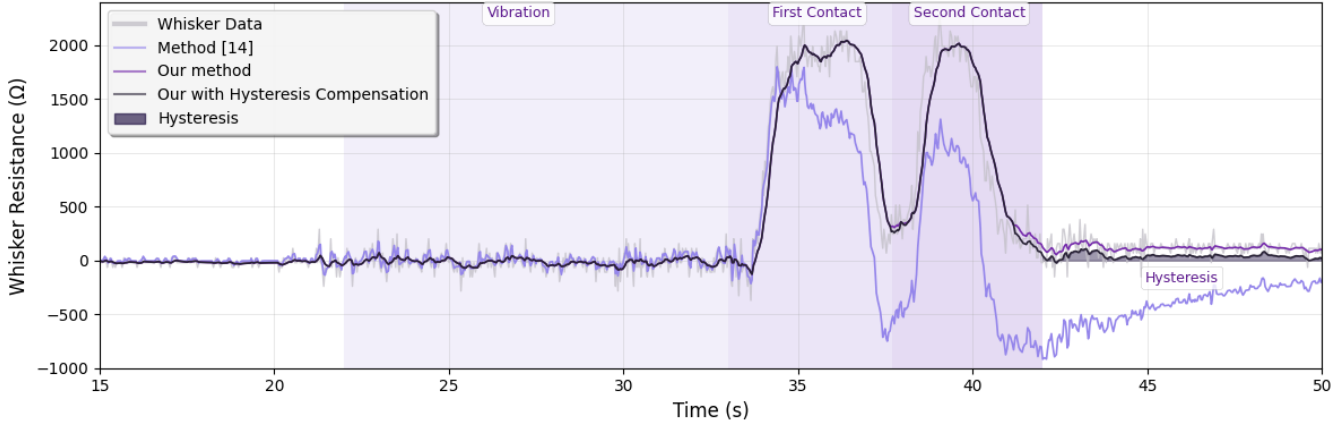
C. System Integration and Signal Processing

The whisker array is mounted directly on the frame of our custom aerial platform. Four flex sensors are hardwired through voltage divider circuits to 12-bit ADS1015 analog-to-digital converters, utilising $47k\Omega$ as fixed resistances in the circuits. Resistance variations in the flex sensors generate corresponding voltage changes, measured via the ADS1015 using equation 1.

$$R_{\text{flex}} = R_{\text{fixed}} * \left(\frac{V_{\text{in}} - V_{\text{measure}}}{V_{\text{measure}}} \right) \quad (1)$$



(a) Non-linearity and hysteresis responses of whisker sensors for contact force and displacement estimation



(b) Comparison of preprocessing steps for whisker sensor reading to address effects of vibration, hysteresis, and creep effect. The experimental setup involves a single whisker sensor mounted on a grounded drone operating at 50% throttle without propellers. The trial consists of two contact events where the drone is manually pushed against a vertical surface and subsequently released. Raw sensor measurements (light gray trace) exhibit baseline noise during the initial period, followed by drone arming and throttle engagement via remote control, two wall contact cycles, and final release. Real-time preprocessing results are displayed following baseline calibration. The purple trace represents a filtering method adapted from literature [15] (implemented on different hardware). The black trace shows our methodology that integrates hysteresis compensation and dynamic baseline adjustment depending on the features of TPU material during the unloading phase, using rate-of-change thresholds.

Fig. 3. (a) Whisker characteristic after calibration with Instron Tensile Testing Machine (b) Signal processing of one whisker sensors after interaction with a vertical wall

where R_{flex} is the varied resistance of flex sensor, R_{fixed} is the fixed resistance, V_{in} is the input voltage of the circuit which is 3.3V, and V_{measure} is the output voltage from ADC.

The ADC interfaces with the Raspberry Pi 3b+ (1.4 GHz 64-bit quad-core ARM Cortex-A53 processor) through TX, RX, and GND connections, configured for maximum sampling at 860 Hz with I2C communication at 50 Hz. All sensor processing, calibration, filtering, and control algorithms are implemented in Python within a ROS2 framework. The Raspberry Pi communicates with the flight controller via UART using MAVROS at 921600 baud to enable high-frequency data transmission from the autopilot. MAVROS additionally provides network routing to QGroundControl for real-time system status visualisation and monitoring.

The whisker sensors are positioned beneath the motors (Figure 2), causing direct vibration to the flex sensors. Coupled with the inherent noise of flex sensors, nonlinear behaviour, hysteresis, and creep effects observed in calibra-

tion tests, we proposed a real-time preprocessing method to mitigate these effects. Initial implementation of a first-order Butterworth bandpass IIR filter (0.03-5.75 Hz) from [15] proved inadequate for transient response during brief contact events because our whisker design experiences more pronounced hysteresis and creep. Building upon their work, we employed a Butterworth low-pass IIR filter tuned to 0.8 Hz to preserve the sudden contact peak features while reducing vibration and sensor noise.

In Figure 3b, we collected the resistance signal when the bumper drone is operating at 50% throttle without propellers. Two contact events were performed against a vertical surface followed by release. While the low-pass IIR filter reduces vibration and noise, the hysteresis and creep remain in our signal response. We calculated a new baseline $\Omega_{i,t}$ for hysteresis and creep compensation following post-contact event. From Section II-B, our calibration analysis revealed that post-contact resistance falls within 3% of the

initial resistance baseline. If the resistance signal exceeds this threshold and the resistance change rate falls in our transition band, we classify this as a post-contact event and trigger the new baseline calculation as shown in equation 2.

$$\Omega_{i,t} = w_t * \Omega_{i,t-1} + (1 - w_t) * LPF(\Omega_t) \quad (2)$$

where, $\Omega_{i,t}$ is the new baseline of whisker sensors, $\Omega_{i,t-1}$ is the previous baseline of whisker sensors, w_t denotes as a weight for baseline calculation, and $LPF(\Omega_t)$ is the result from the first-order Butterworth band-pass IIR filter at time step t . We tune our parameter to keep the compensation after contact as much as possible. The weight (w_t) helps prevent baseline oscillation, and is calculated using equation 3.

$$w_t = \begin{cases} 0, & \text{if } |\dot{\Omega}| \leq T_{min} \\ 1, & \text{if } |\dot{\Omega}| \geq T_{max} \\ (1 - \beta) * w_{t-1} + \beta * \varepsilon_t, & \text{if } T_{min} < |\dot{\Omega}| < T_{max} \end{cases} \quad (3)$$

$$\varepsilon_t = \left[\frac{|\dot{\Omega}| - T_{min}}{T_{max} - T_{min}} \right], \varepsilon_t \in [0, 1] \quad (4)$$

where, ε_t denotes as a normalised contact activity level within the transition band, T_{min} denotes as a minimum rate of change of Ω_t , and T_{max} denotes as a maximum rate of change, and β is the weight smoothing. Each parameter is tunable heuristic. Optimized parameters include: $T_{min} = 0 \Omega/\text{sec}$, $T_{max} = 230 \Omega/\text{sec}$, and $\beta = 0.35$. Figure 3b demonstrates that hysteresis compensation activates exclusively during post-contact events and resistance values reach steady-state.

III. EXPERIMENTS

In this section, the flight experiments of the proposed system are presented and discussed. We perform a drone system performance with two experiments: 1) Touch-and-go manoeuvre, 2) Static pushing tasks. The first objective is to demonstrate that our novel platform can perform passive collision recovery using morphological design of our whisker sensors. The second objective is to show that standard low-level controller of Autopilot drone attached with our whisker design can maintain stability when applying normal contact force to a vertical wall.

TABLE I
COMPONENTS FOR WHISKER-INSPIRED AERIAL BUMPER

Frame	HobbyKing™ Totem Q250
Electronic Speed Controller (ESC)	SpeedyBee F7 V3 BL32 50A 4-in-1 ESC
Autopilot	Holybro Kakute H7 Mini V1.5
Firmware	PX4 v1.15.4
Companion Computer	Raspberry Pi 3b+ RAM 1GB (Ubuntu OS server)

A. Experiment setup

The custom-built quadrotor platform comprises components listed in Table III. All propeller guards, landing gear, and battery protection cases are 3D-printed using ABS plastic in accordance with the risk assessment standards of Bristol Robotics Laboratory (BRL). The aircraft has an all-up weight of 700 g. Both experimental trials were conducted within the indoor flight facility at BRL. Safety mattresses were positioned on the floor as protective measures against potential crashes. As shown in Figure 4, the drone was positioned facing the vertical wall for the first experiment and oriented toward the panel surface for the second experiment.

Whisker sensor calibration procedures were completed prior to each experimental run to collect the baseline as described in Section II-B. Following calibration, the aircraft was switched to Stabilised flight mode via RC input. All experiments were conducted manually using the same pilot, including manual arming and manual take-off operations. Control inputs for both experiments were limited to throttle commands for attitude control and pitch inputs for environmental interaction maneuvers. The first experiment involved zeroing pitch inputs immediately upon wall contact, whereas the second experiment maintained continuous pitch commands throughout panel contact phases. All data acquisition was managed through the ROS2 framework running on a Raspberry Pi 3B+. The sampling rate of both the onboard IMU of the flight controller and the IMU topic in MAVROS was set to 100 Hz.



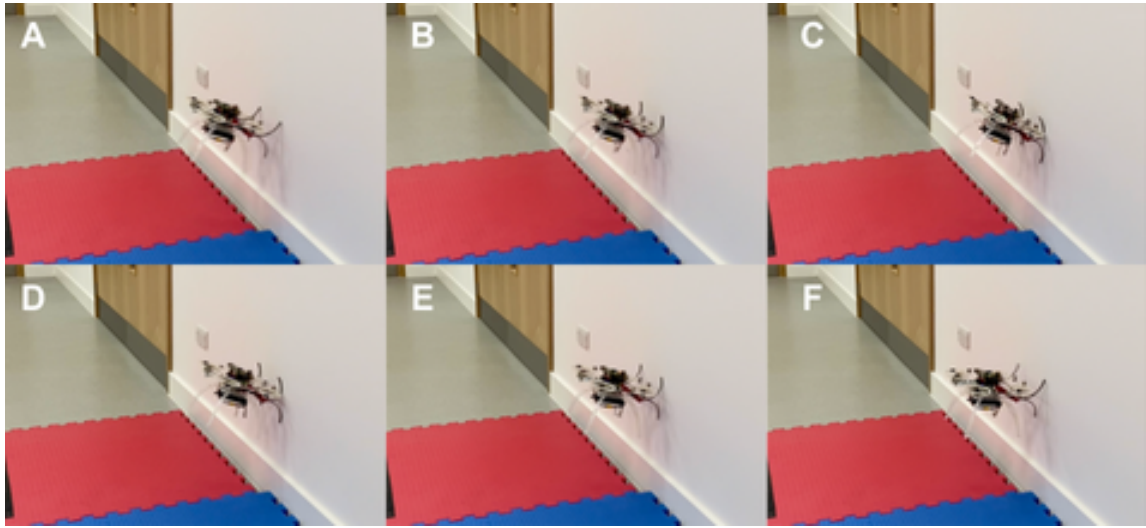
(a) The first experiment setup of Touch-and-go manoeuvre (b) The second experiment setup of Static pushing tasks

Fig. 4. Experimental setups of the bumper drone

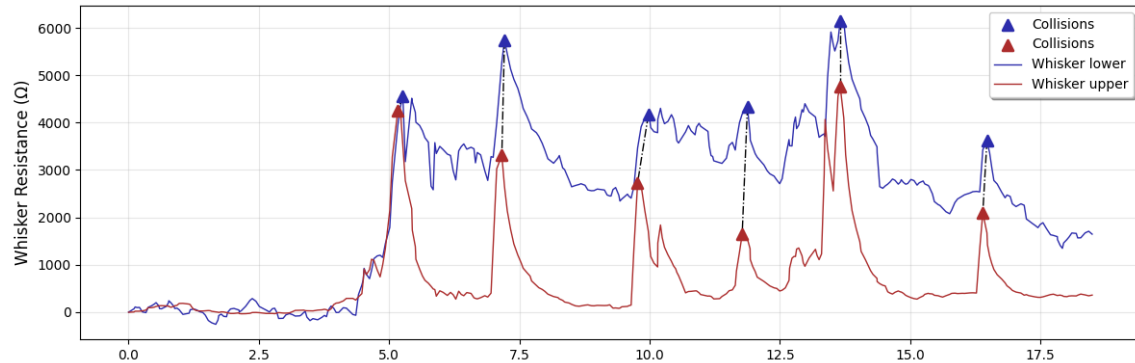
IV. RESULTS

A. Touch-and-go manoeuvre

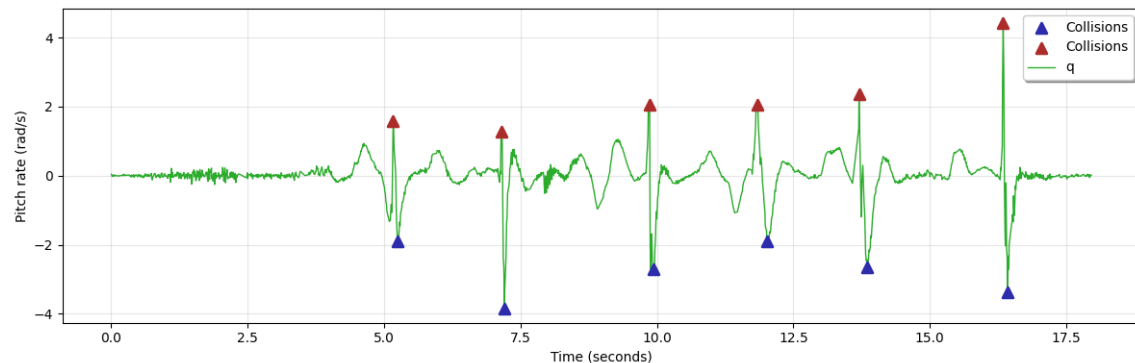
As described in Section II-A, we conducted experiments mimicking the flight behaviour of flying insects during repeated, brief wall interactions. Following take-off to a specified altitude, the bumper drone was controlled exclusively through pitch angle commands via RC input. This experimental setup emulates the scenario where a flying insect already extends its legs for landing but fails to establish stable contact or adhere the vertical wall, resulting in a collision.



(a) The sequence of passive recovery mechanism of the whisker sensors during one collision. (A) The bumper drone is approaching the vertical wall with initial pitch angle of 0.2 rad. (B) Two upper whisker sensors first contact with the wall. (C) Due to collision dynamics, two lower whisker sensors contact with the wall. (D) Four Whisker sensors absorb collision energy. (E) The drone bumper starts to bounce-off. (F) The drone is bounced-off the wall and stabilise. This collision occurs within 200ms. ms



(b) The whisker resistance responses of upper whisker sensors (red) and lower whisker sensors (blue). The plot shows that the upper whiskers contact first and the wall generates a positive pitch angle causing the drone to rotate about the pitch axis, followed by lower whisker sensor contact. The total collision count is 6 occurrences.



(c) The pitch rate of the bumper drone corresponding to the whisker sensor resistance.

Fig. 5. The sequence of events and system response of repeated collision of the bumper drone.

Figures 5b and 5c demonstrate the sequential contact mechanism during collision events throughout one flight experiment experiencing 6 collisions in total. Figure 5b shows the whisker sensor resistance, where the red line represents the filtered resistance of the upper whisker and the blue line

represents the lower whisker resistance. The red triangles indicate maximum resistance following upper whisker contact events, whilst the blue triangles indicate maximum resistance of the lower whisker. After full deformation of the upper whisker, the lower whisker passively establishes contact

within an average of 80ms due to the collision dynamics. The upper whisker exhibits sharp resistance spikes, while the lower whisker shows more gradual resistance changes that take longer to return to baseline, suggesting a damping role with slower recovery dynamics that help absorb collision impact.

This sequential contact pattern is further supported by the pitch rate response shown in Figure 5c. During each collision, initial upper whisker contact generates a positive moment producing an upward pitch rate spike until the upper whiskers are fully deformed (red triangles), immediately followed by a sharp negative pitch rate as the lower whiskers establish contact and undergo deformation (blue triangles). The pronounced negative dip demonstrates the rotational dynamics during collision, with pitch rate gradually returning to neutral as the bumper drone disengages. The consistency of this positive-then-negative pattern of pitch rate across multiple collision events, combined with the resistance data, demonstrates the passive collision recovery of our whisker design.

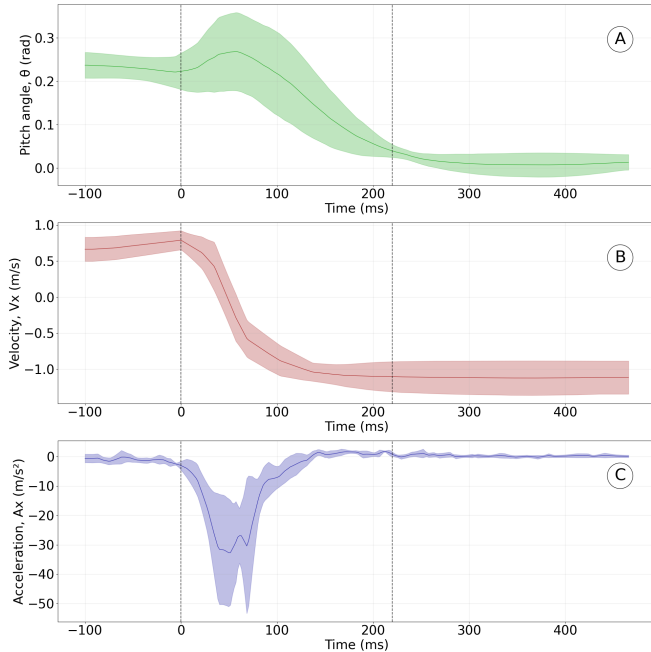


Fig. 6. These plots show the average and variance of pitch angle, velocity body in x-axis, and linear acceleration in x-axis before and after collisions. The collision occurs at $t = 0$, with a sudden velocity change and $t = 219$ ms when represents when velocity becomes stable again, representing the average collision duration (A) Pitch angle plots. The pitch angle increases by approximately 0.05 rad following collision and returns to neutral pitch angle. (B) Speed decreases in a cubic profile from 0.78 m s^{-1} to -1.12 m s^{-1} on average. (C) Average linear acceleration plots. Linear acceleration remains relatively constant after collision with a spike during the collision event, reaching 50 m s^{-2} . Note the sudden drop and rise in linear acceleration when the lower whisker sensor contacts the wall.

Moreover, the repeatability of the platform was tested across 17 collisions conducted over 3 flight experiments. Figure 6 plots show the pitch angle, forward velocity (V_x), and forward acceleration (A_x) during a single collision event, averaged across all flight experiments. The shaded regions

TABLE II
OSCILLATIONS OF THE UAV ON THE ATTITUDE

RMS	Mean (rad)	STD (rad)
Pitch (θ)	0.072	0.23
Roll (ϕ)	0.013	0.08

represent the standard deviation across these collisions. Two vertical dashed lines at $t = 0$ ms and $t \approx 219$ ms correspond to the initial contact and end of contact event. The temporal responses exhibit characteristics similar to a mass-spring-damper system. The pitch angle (A) demonstrates a smooth exponential decay typical of an overdamped response, while the velocity profile (B) shows the characteristic step response with rapid deceleration followed by gradual recovery. The acceleration trace (C) captures the impulse-like response at impact, with a sharp negative spike followed by oscillatory recovery. The stability of the bumper drone during collision interactions is assessed by analysing attitude oscillations. The amplitude of oscillations is calculated using the root mean square (RMS) of the roll angle (ϕ) and pitch angle (θ) as shown in Table II. The results demonstrate low pitch oscillations showing an RMS value of only 0.072rad (4°) and roll oscillations of just 0.013rad (0.74°).

B. Static pushing tasks

The static pushing experiments were conducted in three phases as illustrated in Figure 7: target approach and contact, sustained contact, and contact release. The drone was commanded using only forward and backward pitch inputs via RC control without any control algorithm used in this experiment. During contact operations, the drone maintained forward contact using pitch commands, while roll and yaw inputs remained neutral values.

Figure 8a presents the orientation of the bumper drone with the maximum pitch angle of 0.35 rad. After the drone was commanded to a specific pitch angle at 0.2 rad, the pitch input remained almost constant to maintain the contact. The plot shows the pitch angle exhibits spring-damped characteristic behaviour inherent to the whisker morphology, oscillating between 0.16 rad (9°) and 0.35 rad (20°). This response demonstrates force absorption provided by the compliant whisker mechanism. However, sustained contact introduces disturbances in the yaw axis, causing the drone to oscillate from -0.15 rad (-8.5°) to 0.2 rad (11°). This indicates that while the whisker design effectively manages pitch-direction forces, some lateral disturbances remain present during contact operations.

We further evaluate system performance under increased loading conditions. We command larger pitch angles up to 0.7 rad (40°) (Figure 8b). Despite the two-times increase in commanded pitch angles, the system maintains the spring-damped behaviours with bound responses between 0.16 rad (9°) and 0.71 rad (40.6°). Yaw oscillations remain within a similar range (-0.15 rad to 0.3 rad). However, at $t \approx 32$, the yaw angle tends to increase as the contact time increases.

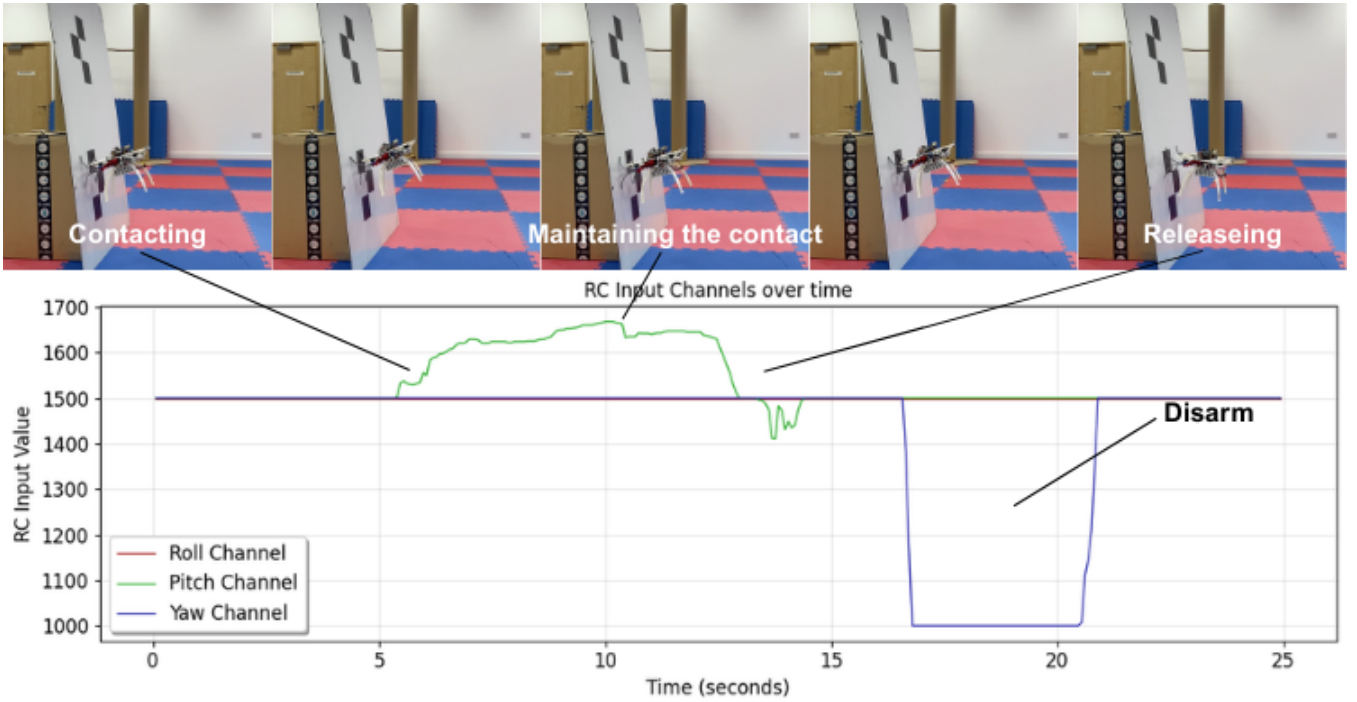


Fig. 7. The sequences of the static pushing task experiment. The video frames are shown, and the RC input channels are plotted. Roll and Yaw channels remain neutral while Pitch channel increases from 1500 to 1650 PWM. This indicates that the bumper drone is commanded only forward motion to maintain contact with the wall.

To investigate the cause of persistent yaw oscillations, we hypothesised that apart from environmental disturbances, the standard PX4 PID rate controllers might contribute to the observed disturbances through integral windup or steady-state error compensation during contact. We conducted comparative experiments using PD-only control by zeroing the integral gains (`MC_ROLLRATE_I`, `MC_PITCHRATE_I`, `MC_YAWRATE_I = 0`).

The results (Figure 8c) show pitch oscillations ranging from 0.2 rad (11°) to 0.85 rad (48°), with yaw disturbances increasing from 0.2 rad (11°) to 0.5 rad (28°) over the contact duration. The elimination of integral gain did not significantly reduce the yaw coupling. Moreover, the increase in yaw oscillation makes only one whisker sensor contact the panel, causing the drone to slip and slide down along the panel. Notably, comparison with literature results [19] shows that similar pitch angles (0.3 rad) produced yaw oscillations from -0.15 rad to 0.4 rad with eventual instability in rigid aerial manipulation systems. This comparison validates that our compliant whisker design provides better disturbance rejection compared to rigid end-effector approaches, even without contact force control algorithms.

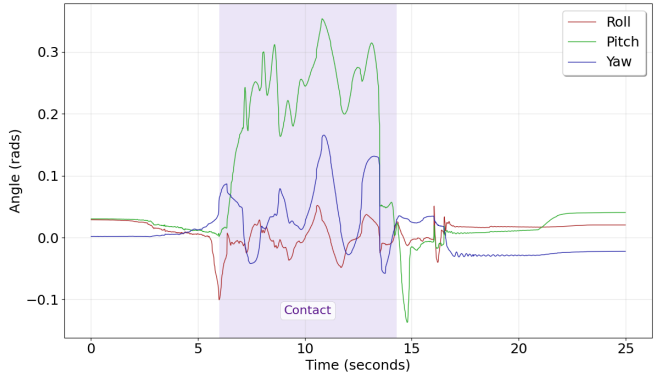
V. DISCUSSION AND CONCLUSIONS

In this work, we designed a whisker-inspired bumper drone toward tactile navigation and static pushing tasks. We analysed our whisker morphology and identified characteristic responses including nonlinearity, hysteresis, and creep effects from the soft, flexible material. We introduced real-time preprocessing steps to mitigate these effects. By combining

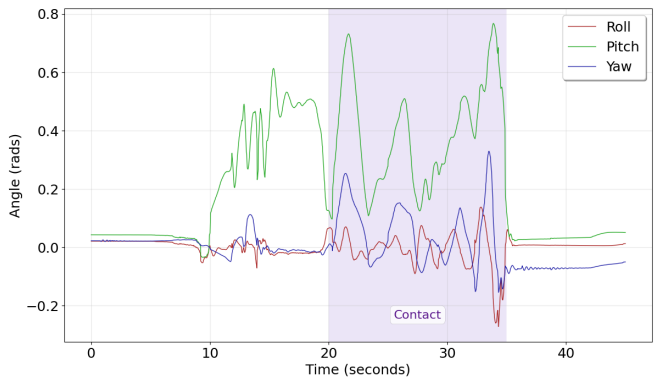
biomimetic whisker morphology with flying insect reflex-landing behaviour, we demonstrated self-recovery mechanisms from collision events, where our whisker design acts as an embodied mass-spring-damper system. Our bumper drone equipped with whisker sensors can absorb impact energy from collisions and maintain vehicle stability, achieving minimal attitude disturbances with pitch oscillations of only 4° and roll oscillations of just 0.74°. Additionally, we showed that stable contact force exertion can be achieved with minimal control effort. By applying pitch RC commands corresponding to 20° and 40° tilt angles, the system maintained stable operation within yaw angles from -8° to 28° and pitch angles from 9° to 48°. This work represents the first demonstration of E-APHI that integrates morphological design and tactile sensing to achieve both active and passive physical interaction behaviours. We demonstrated that our bumper drone can simplify control policies and potentially enhance performance in unpredictable natural environments, paving the way for applications in exploration of poorly lit conditions and GPS-denied environments.

A. Limitations

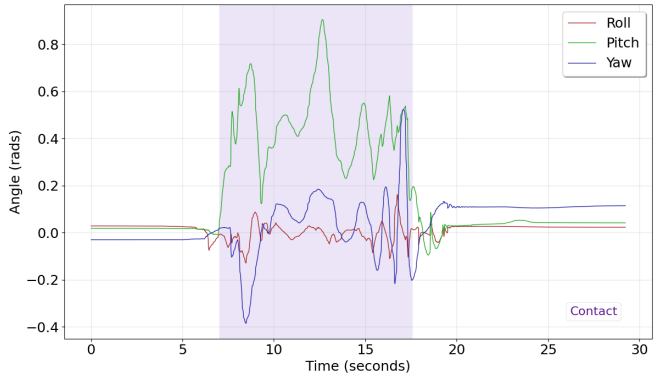
1) *Systematic Whisker Sensor Bias:* The primary limitation of our whisker design lies in systematic bias arising from sensor failures such as physical damage and electrical wire degradation. Apart from actual flight experiments, endurance testing involving 20 consecutive wall collisions demonstrated that whisker sensors suffer structural damage gradually that affects measurement accuracy and reliability. The electrical wires connected to flex sensors become loosened due to



(a) Orientation of UAV with maximum pitch of 0.35 rad



(b) Orientation of UAV with maximum pitch of 0.7 rad



(c) Orientation of UAV without I gain from rate controller

Fig. 8. Orientation of UAV in the static pushing task experiment. The yaw angle oscillates in a small region and even oscillates more if the pitch angle increases, corresponding to an increase in contact force.

repeated collision impacts, rendering the ADC readings invalid. While our bumper drone retains collision capability following sensor failures, the flex sensor readings become increasingly unreliable. Although this systematic bias has not been clearly observed in our current experiments due to the absence of closed-loop control algorithms incorporating tactile feedback, this issue represents a fundamental challenge for autonomous operation. Sensor degradation could lead to erroneous readings that trigger unexpected flight behaviour, potentially compromising system safety and mission reliability.

2) Limited Operational Range: The current whisker configuration exhibits critical geometric constraints that limit operational effectiveness. The bumper drone suffers from restricted operational range, particularly when encountering obstacles insufficient in width to engage both whisker sensors simultaneously. In such scenarios, the system experiences collision without detection capability, representing a critical hazard for autonomous operations. This limitation stems from the discrete four-whisker arrangement, which creates sensing gaps that could be exploited by small or oddly shaped obstacles. In addition, the current design lacks omnidirectional sensing capability, constraining the system's ability to interact with diverse surface geometries and limiting its applicability to complex environments.

B. Future work

1) Whisker design parameters: Our whisker sensors were designed based on biological inspiration, leaving room for further optimisation. We can explore varied geometries and materials to investigate changes in stiffness and damping coefficients. With different combinations of stiffness and damping properties, we can study the relationship between these parameters in single collision events, monitoring energy dissipation and absorption. We could potentially identify the elastic and plastic deformation regions and failure points that reduce systematic bias and guarantee resistance reading accuracy. Through energy dissipation observations, we can vary the approaching velocities and determine the optimal parameters for collision behaviour.

2) Sensor Calibration Model: In reality, several factors affect flex sensor readings, including contact position (related to drone pitch angle during flight), contact surface friction, and drone velocity and acceleration. Extending the calibration setup by fusing IMU data from the drone during flight could potentially increase flex sensor reading accuracy. The overall system could more effectively detect lateral drone movements, thereby establishing baseline experiments for sliding tasks to compare with our touch-and-go movements. We could adopt the procedure described in [20] that fuses flex sensor readings with an Unscented Kalman Filter (UKF) and applies learning-based methods using Long-Short-Term-Memory (LSTM) neural networks or Recurrent Multi-output Networks (RMN) [15] for time-series data prediction to estimate contact forces and displacement with flex sensors.

3) Toward Autonomous Navigation: Having demonstrated manual control of pitch angle for touch-and-go manoeuvres, we can generate automated pitch profiles to enable autonomous wall collisions. We can adjust pitch angle magnitude, collision duration, and inter-collision periods, similar to Pulse Width Modulated (PWM) signals. Between collisions, assuming a large wall surface, we could adjust the roll angle incrementally and apply the pitch profile repeatedly, creating a simple navigation planner. With an accurate whisker sensor model, we can predict sensor deformation and estimate deformation using approach velocity and pitch angle to determine expected normal contact forces from each whisker. This information enables estimation of pre-

and post-collision distances in the orthogonal direction and calculation of balance forces between left and right whiskers to infer wall orientation, progressing toward autonomous tactile navigation. Since we employ rate controllers, our bumper drone can perform autonomous navigation without relying on external position estimation systems. Furthermore, whisker sensing can inform simple PD controllers using the summation of resistance from both upper whiskers to control pitch angle and the difference between upper whiskers to control yaw angle. This approach would enable our bumper drone to push dynamic and static objects with lower oscillation.

REFERENCES

- [1] F. Ruggiero, V. Lippiello, and A. Ollero, "Aerial manipulation: A literature review," *IEEE Robotics and Automation Letters*, vol. 3, no. 3, pp. 1957–1964, 2018.
- [2] D. Lee, H. Seo, D. Kim, and H. J. Kim, "Aerial manipulation using model predictive control for opening a hinged door," 2020. [Online]. Available: <https://arxiv.org/abs/2003.08256>
- [3] X. Meng, Y. He, Q. Li, F. Gu, L. Yang, T. Yan, and J. Han, "Contact force control of an aerial manipulator in pressing an emergency switch process," in *2018 IEEE/RSJ International Conference on Intelligent Robots and Systems (IROS)*, 2018, pp. 2107–2113.
- [4] H. Seo, S. Kim, and H. J. Kim, "Aerial grasping of cylindrical object using visual servoing based on stochastic model predictive control," in *2017 IEEE International Conference on Robotics and Automation (ICRA)*, 2017, pp. 6362–6368.
- [5] H. Chen, W. Deng, B. Ye, Y. Xiong, Z. Pan, and X. Lyu, "Aerial grasping via maximizing delta-arm workspace utilization," 2025. [Online]. Available: <https://arxiv.org/abs/2506.15539>
- [6] X. Guo, G. He, M. Mousaei, J. Geng, G. Shi, and S. Scherer, "Aerial interaction with tactile sensing," in *2024 IEEE International Conference on Robotics and Automation (ICRA)*, 2024, pp. 1576–1582.
- [7] W. Zhang, L. Ott, M. Tognon, and R. Siegwart, "Learning variable impedance control for aerial sliding on uneven heterogeneous surfaces by proprioceptive and tactile sensing," *IEEE Robotics and Automation Letters*, vol. 7, no. 4, pp. 11 275–11 282, 2022.
- [8] K. Bodie, M. Brunner, M. Pantic, S. Walser, P. Pfändler, U. Angst, R. Siegwart, and J. Nieto, "Active interaction force control for contact-based inspection with a fully actuated aerial vehicle," *IEEE Transactions on Robotics*, vol. 37, no. 3, pp. 709–722, 2021.
- [9] X. Guo, G. He, J. Xu, M. Mousaei, J. Geng, S. Scherer, and G. Shi, "Flying calligrapher: Contact-aware motion and force planning and control for aerial manipulation," *IEEE Robotics and Automation Letters*, vol. 9, no. 12, pp. 11 194–11 201, 2024.
- [10] S. Hamaza, I. Georgilas, and T. Richardson, "2d contour following with an unmanned aerial manipulator: Towards tactile-based aerial navigation," in *2019 IEEE/RSJ International Conference on Intelligent Robots and Systems (IROS)*, 2019, pp. 3664–3669.
- [11] A. Bredenbeck, C. D. Santina, and S. Hamaza, "Embodying compliant touch on drones for aerial tactile navigation," *IEEE Robotics and Automation Letters*, vol. 10, no. 2, pp. 1209–1216, 2025.
- [12] R. Wang, Z. Guo, Y. Chen, X. Wang, and B. M. Chen, "Air bumper: A collision detection and reaction framework for autonomous mav navigation," in *2024 IEEE International Conference on Robotics and Automation (ICRA)*, 2024, pp. 15 735–15 741.
- [13] Z. Liu and K. Karydis, "Toward impact-resilient quadrotor design, collision characterization and recovery control to sustain flight after collisions," in *2021 IEEE International Conference on Robotics and Automation (ICRA)*, 2021, pp. 183–189.
- [14] E. Aucone and S. Mintchev, "Embodied aerial physical interaction: Combining body and brain for robust interaction with unstructured environments," *Science Robotics*, vol. 10, no. 102, p. eads0200, 2025. [Online]. Available: <https://www.science.org/doi/abs/10.1126/scirobotics.ads0200>
- [15] C. Ye, G. De Croon, and S. Hamaza, "A biomorphic whisker sensor for aerial tactile applications," in *2024 IEEE International Conference on Robotics and Automation (ICRA)*, 2024, pp. 5257–5263.
- [16] H. Li, C. Xing, S. Khan, M. Zhong, and M. R. Cutkosky, "Whisker-inspired tactile sensing: A sim2real approach for precise underwater contact tracking," *IEEE Robotics and Automation Letters*, vol. 10, no. 6, pp. 6087–6094, 2025.
- [17] M. A. Lin, E. Reyes, J. Bohg, and M. R. Cutkosky, "Whisker-inspired tactile sensing for contact localization on robot manipulators," 2022. [Online]. Available: <https://arxiv.org/abs/2210.12387>
- [18] A. Briod, "Observation of insect collisions," 2008. [Online]. Available: <https://infoscience.epfl.ch/handle/20.500.14299/92749>
- [19] H. W. Wopereis, J. J. Hoekstra, T. H. Post, G. A. Folkertsma, S. Stramigioli, and M. Fumagalli, "Application of substantial and sustained force to vertical surfaces using a quadrotor," in *2017 IEEE International Conference on Robotics and Automation (ICRA)*, 2017, pp. 2704–2709.
- [20] A. Tagliabue, A. Paris, S. Kim, R. Kubicek, S. Bergbreiter, and J. P. How, "Touch the wind: Simultaneous airflow, drag and interaction sensing on a multirotor," in *2020 IEEE/RSJ International Conference on Intelligent Robots and Systems (IROS)*, 2020, pp. 1645–1652.